Journal of Applied Physics ARTICLE scitation.org/journal/jap

Ultrafast imaging of surface-exclusive carrier dynamics in silicon

Cite as: J. Appl. Phys. **125**, 185303 (2019); doi: 10.1063/1.5074198
Submitted: 22 October 2018 · Accepted: 22 February 2019 ·
Published Online: 10 May 2019

View Online Export Citation CrossMark

Ebrahim Najafi[1,a)] and Amir Jafari[2]

AFFILIATIONS

[1]Chemistry and Chemical Engineering Division, California Institute of Technology, 1200 E. California Blvd, Pasadena, California 91125-0002, USA
[2]Department of Physics and Astronomy, Johns Hopkins University, Baltimore, Maryland 21218, USA

[a)]**Author to whom correspondence should be addressed:** enajafi@caltech.edu. **Present address:** DuPont Experimental Station, 200 Powder Mill Rd, Wilmington, Delaware, USA.

ABSTRACT

Understanding the dynamics of charge carriers at the semiconductor surfaces and interfaces is fundamental to the further development of photocatalytic, photovoltaic, and optoelectronic devices. Here, we study the surface photovoltage (SPV) dynamics in intrinsic and doped silicon using scanning ultrafast electron microscopy (SUEM). SUEM is a surface sensitive technique that allows the direct imaging of carriers at ultrafast time scales, thereby elucidating their spatiotemporal response to optical excitation. We first discuss the mechanism of image formation in SUEM. We then use these images to show that carrier dynamics on the silicon surface depends strongly on the doping type and concentration, though not always dictated by SPV. The numerical simulation of the drift-diffusion model suggests that this is due to the formation of complex transport processes, driven by intrinsic and photoinduced fields in the excited volume. This work refines our current understanding of the surface-exclusive dynamics in semiconductors by introducing a means to study their evolution in space and time and providing a model to explain the underlying mechanism.

I. INTRODUCTION

The optical excitation of semiconductors with sufficiently energetic photons leads to the generation of free electron-hole pairs across the bandgap. The relaxation pathway of these nonequilibrium carriers involves the exchange of energy, transport in the space, and complete disappearance due to recombination. The control and manipulation of these events, whose time scales span from a few femtoseconds to hundreds of microseconds,[1] will facilitate the efficient conversion of the solar energy into electricity or its storage into chemical bonds.

Charge carrier dynamics are fundamental to the energy loss and scattering processes in semiconductors. Such dynamics are generally characterized by optical pump-probe spectroscopy, which conventionally measures the transient reflectivity or transmission of the sample following an abrupt excitation by an optical pulse.[2,3] This allows the investigation of the intermediate pathways that carriers undertake, including energy and momentum normalization, carrier-phonon scattering, diffusion, and recombination.[1,3] Although carrier dynamics in bulk semiconductors are fully understood, those that take place at the surfaces and interfaces as well as in nanomaterials remain an enigma. This is primarily due to the poor spatial resolution of the optical probe, which limits the examination of submicron features. In addition, because of the large penetration depth of the visible light in semiconductors, the signal generated in the bulk often masks the surface contribution.

As modern devices miniaturize into the nanoscale regime, their surface area substantially increases; therefore, a clear understanding of the interfacial carrier dynamics becomes essential for their operation and output.[4–6] With the recent development of scanning ultrafast electron microscopy (SUEM), we are now able to "directly" image carriers and follow their progression from the excited state toward the ground state.[7–13] While there is a growing body of literature on the design and application of SUEM, only a little work has been dedicated toward understanding the origin of the recorded signal and the contrast mechanisms; this often leads to the misinterpretation of the dynamics especially in systems driven far away from equilibrium.

Here, we report the SUEM imaging of the surface photovoltage (SPV) dynamics in silicon and explain how this process is manifested in the recorded images. SPV, which is the response of the surface potential to the temporary repopulation of the surface states by photoexcited carriers, characterizes the electronic properties of semiconductors.[14,15] In this study, we measure the rise and the decay time scales of SPV in intrinsic and doped silicon by recording the relative intensity of the transient SE emission since it directly reflects the variations in the surface barrier potential. SUEM's surface sensitivity results in a better understanding of the "actual" surface processes by simply eliminating the contributions of the underlying bulk. We observe that the intensity as well as the rise and the decay time scales of the signal depend strongly on the doping type and concentration, but not necessarily as expected from SPV. For instance, we see similar surface dynamics in lightly doped n-type and p-type silicon, despite their different surface characteristics. We then build a numerical model to describe this behavior. We show that optical excitation generates complex transport processes in the subsurface, due to the formation of strong fields in the excited volume, which, in return, strongly impact the surface dynamics. Our observation provides new insights into the origin of the spatial dynamics of carriers at the top few nanometers of the semiconductor surface, a knowledge essential for the operation optimization of the optoelectronic, photocatalytic, and photovoltaic devices, especially as they further miniaturize into the nanoscale regime; such a valuable insight is only obtained using ultrafast microscopy techniques, such as SUEM, that probe carriers in space and time.

II. EXPERIMENTAL METHOD

For this experiment, intrinsic and doped silicon samples were purchased from MTI Corp. and used without any chemical functionalization (see the complete list in Table I). The doping types and concentrations were further evaluated by energy dispersive X-ray spectroscopy. The samples were cleaved and immediately transferred into the SUEM chamber where the vacuum was maintained at 2×10^{-7} Torr. Surfaces with the root mean square roughness of less than 100 nm, orders of magnitude smaller than the estimated diffusion length in silicon, were selected for this experiment to minimize interruptions in carrier diffusion.[16] The design and operation of SUEM were explained previously, but a short description follows. SUEM consists of a conventional SEM combined with a laser source (IMPULSE by Clark-MXR), which produces femtosecond IR pulses (300 fs, 1030 nm). These pulses are split to produce green (515 nm) and UV (257 nm) pulses through harmonic generation. The former is guided into SUEM through a transparent window to excite samples at an elliptical crossover (diameters 30 μm and 50 μm), while the latter is directed toward the photocathode to produce short electron pulses from the field emission tip. The time delay between the green and electron pulses is synchronized by a mechanical stage, which provides 3.3 ns interval at 1 ps steps. The electron pulses are then accelerated to 30 kV and focused on the sample by electrostatic lenses to produce secondary electrons (SEs), which are then collected by the SE detector and converted into pixel intensities in the image. To form an image at a particular time delay, the surface was scanned by the electron probe focused into a 200 nm spot, which was sufficient to capture spatial details in this study. To remove the background contribution and enhance the dynamic signal, the image of the sample in the ground state ($t \ll 0$) was subtracted from the dynamic images recorded after optical excitation ($t \geq 0$). This produced so-called "contrast images," in which the bright and dark signals were interpreted as increases in electron and hole densities, respectively. Although the number of SEs emitted from the surface depends on a few factors including chemical composition and topography,[17,18] the subtraction of the reference image ensures that such parameters are eliminated from the contrast images and the signal becomes representative of only the changes in the carrier density.

III. RESULTS AND DISCUSSIONS

Figure 1 shows the schematic of the experiment, where the green pulse excites the sample and the electron pulse raster scans the surface and measures the dynamics. When the sample is in the ground state, the thermal equilibrium between the surface and the bulk induces the space-charge region (SCR) with bent electronic bands in the subsurface; therefore, free carriers have to overcome the resulting barrier potential (V_s) before they further occupy the surface.[19] Naturally, band bending is negligible in intrinsic and lightly doped silicon but increases significantly when the doping concentration approaches the degeneracy threshold.[18] The super-bandgap excitation of the surface with the green pulse generates large densities of free electrons (n_e^*) and holes (n_h^*) in the subsurface. These carriers are subsequently separated by the SCR and drifted in opposite directions, where the majority carriers are transported into the bulk and the minority carriers toward the surface. As charge separation completes, the electronic bands somewhat flatten which, in return, reduces V_s.

In general, SUEM, similar to SEM, probes the surface by recording the total SE yield (δ) as the primary electrons inelastically interact with the sample. In the SE emission process, δ depends on the number of electrons excited by the primary beam at distance z below the surface, E_0/ϵ, the probability of these electrons to reach

TABLE I. Intrinsic and doped silicon samples selected for the current study together with the fitting parameters of the observed dynamics.

Sample	Doping concentration	Time constants of exponential fits
Intrinsic	...	$\tau_1 = 6$ ps, $\tau_2 = 4$ ps, $\tau_3 = 176$ ps, $\tau_4 = 20$ ns
Lightly doped n-type	2.6×10^{15} P/cm^3	$\tau_1 = 5$ ps, $\tau_2 = 4$ ps, $\tau_3 = 146$ ps, $\tau_4 = 6.5$ ns
Heavily doped n-type	1.9×10^{19} P/cm^3	$\tau_2 = 77$ ps, $\tau_3 = 10$ ps, $\tau_4 = 5.2$ ns
Lightly doped p-type	3.8×10^{15} B/cm^3	$\tau_2 = 5$ ps, $\tau_3 = 148$ ps, $\tau_4 = 6.5$ ns
Heavily doped p-type	2.2×10^{19} B/cm^3	$\tau_2 = 58$ ps, $\tau_3 = 36$ ps, $\tau_4 = 4.7$ ns

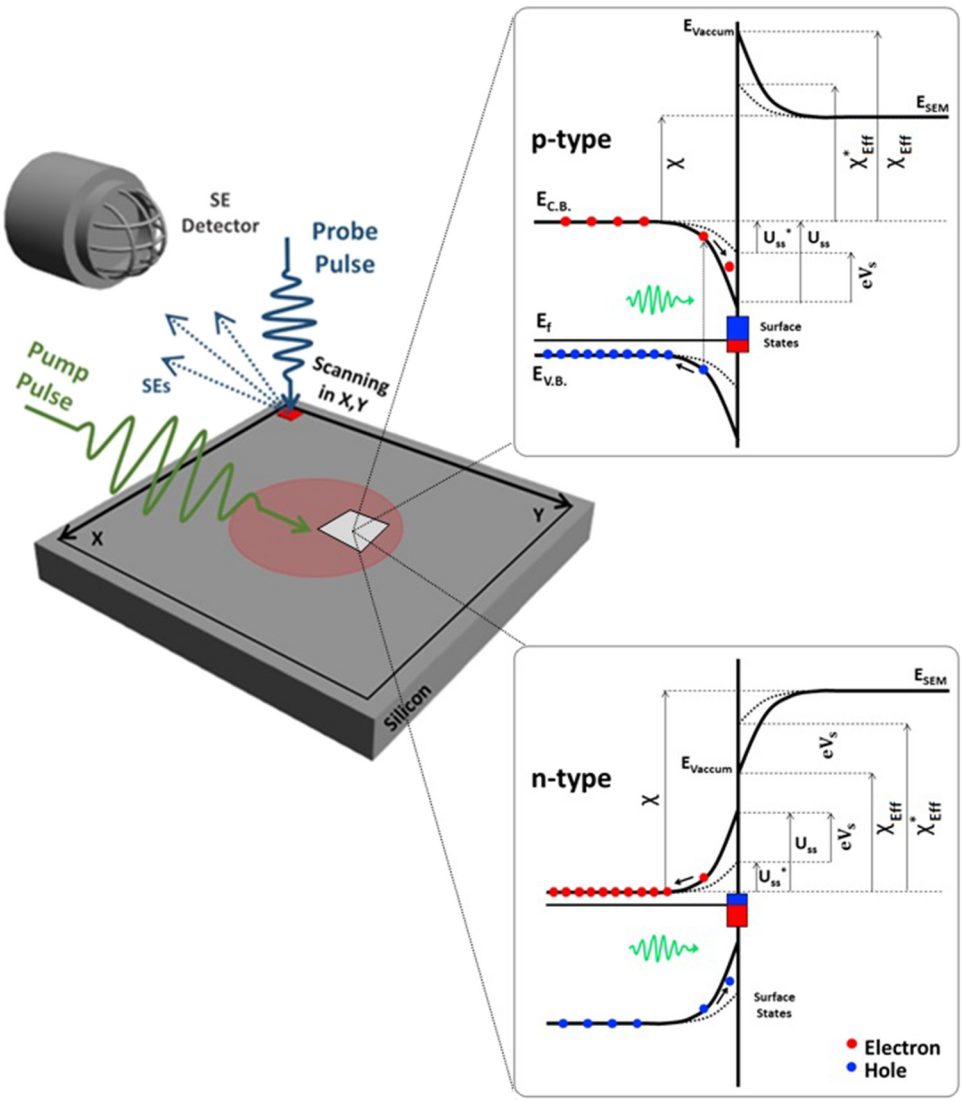

FIG. 1. Schematic depiction of the experimental setup where the green pulse excites the sample, while the electron pulse probes the dynamics by scanning the surface and generating SEs. In the doped silicon, the thermal equilibrium between the bulk and the surface can lead to a significant band bending in the subsurface. The photoexcitation of these samples results in the transport of the minority carriers toward the surface and the majority carriers into the bulk due to the presence of the built-in potentials. This dynamically changes the electron affinity (χ) at the surface, and thus the height of the barrier potential (V_s). Since the SE emission depends strongly on χ, SPV results in substantial changes in SE emission in the illuminated region relative to the surrounding.

the surface, $e^{\beta z}$, and the probability of their escape into the vacuum, B,[19–22,23,24]

$$\delta = \frac{E_0}{\epsilon} B e^{-\beta r}, \tag{1}$$

where E_0 is the energy of the primary electrons, ϵ is the average energy required to generate an electron-hole pair, r is the distance from the surface where pairs are generated, and β is a material dependent constant. For electrons arriving at the surface with an isotropic velocity distribution and energy E, B is determined by the electron affinity χ,[19–22,23,24]

$$B(E) = 1 - \left(\frac{\chi}{E}\right)^{1/2}. \tag{2}$$

Thus, it becomes easier for free electrons to reach the surface and emit as SEs when χ decreases (Fig. 1). In other words, the SE emission depends on χ and V_s, which, in turn, are determined by the net carrier density $(n_e^* - n_h^*)$ on the surface. Consequently, from the photoexcited region of p-type silicon, more SEs are collected since the net carriers locally reduce χ and V_s. Conversely, less SEs are collected from the same region of n-type silicon since the net carriers locally increase χ and V_s.

Figure 2(a) shows the dynamic behavior of the intrinsic silicon after optical excitation. In the negative time ($t = -50$ ps), the sample shows no observable contrast since it exists in the ground state. Following optical excitation, a bright contrast emerges at the laser-sample crossover, due to the increased SE emission. The intensity of the bright contrast increases systematically with time and appears to maximize by approximately 10 ps. However, the signal is rather weak with the spatial extent similar to that of the laser profile; such a weak excitation in the intrinsic silicon in expected due to its indirect bandgap which makes the transition a second-order process.

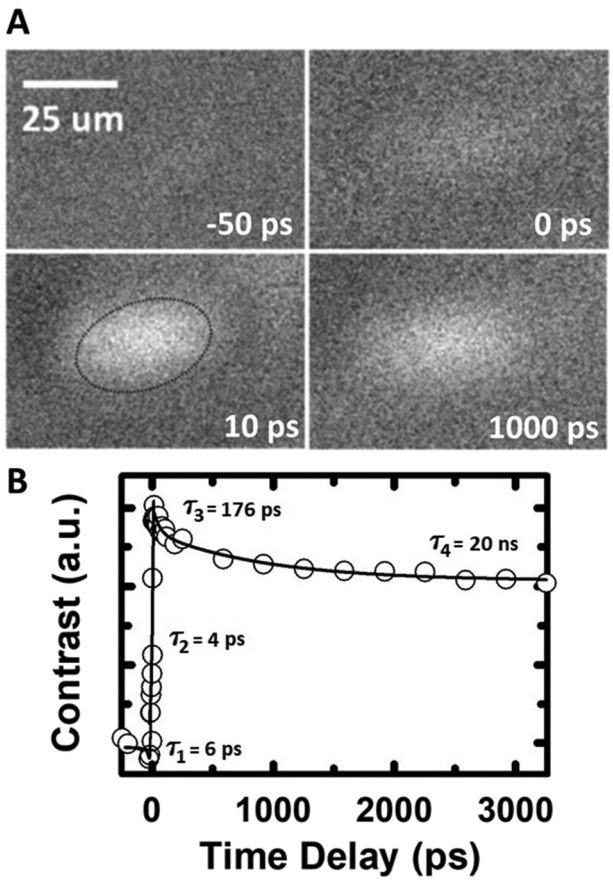

FIG. 2. (a) SUEM images of the intrinsic silicon recorded before ($t = -50$ ps) and after optical excitation ($t > 0$ ps). The images indicate an increase in the SE emission from the surface as evident from the emergence of the bright contrast. The contrast gradually diminishes at later times as the sample retrieves the ground state. (b) Contrasts extracted from the photoexcited region [dotted ellipse in Fig. 2(a)] and plotted vs time delays.

Furthermore, a dark halo develops around the bright contrast as shown in the low magnification image in Fig. S1 in the supplementary material. This suggests that the intrinsic free carriers in the neighborhood are involved in a process that runs parallel to that in the crossover. After the termination of the laser pulse, the sample gradually returns to the ground state as evident from the decrease in the bright contrast. Figure 2(b) plots the contrasts, averaged over the dotted ellipse in Fig. 2(a), vs time delays (solid circles). The graph shows further details in the dynamics, which include a negative signal after optical excitation which quickly transitions into a sharp positive followed by a fast and a subsequent slow recovery as the system returns to the ground state. The time constant of the dark contrast was determined to be 6 ps. Similarly, the time constants of the rise and the decays of the brightness are also determined from the exponential fit to be 4 ps, 176 ps, and 20 ns (Table I). The slow recovery agrees with previously reported time scales for the carrier recombination in silicon.[25]

Figure 3 shows the SUEM images recorded from the surfaces of doped silicon samples. In all cases, there are no observable dynamics in the negative time, indicative of the fast recovery within 200 ns between two consecutive pulses. In addition, after optical excitation, the images display bright signals in lightly doped p-type (A) and n-type (B) as well as in heavily doped p-type (C) samples, which correspond to the localized increases in the SE emission. In contrast, heavily doped n-type silicon (D) shows a dark signal, due to the localized decrease in the SE emission. The observation of the bright signal in lightly doped n-type is surprising since SPV is expected to increase the hole density on the surface, thereby increasing the surface barrier potential. In all these cases, the intensity and the spatial extension of the signals are larger than those in the intrinsic silicon and increase systematically as the doping level increases. This is because of the bandgap narrowing in doped samples that increases the absorption cross section.[26] Similar to the intrinsic silicon, the low magnification images show a dark halo surrounding the photoexcited regions in the lightly doped n-type; this is indicative of an underlying mechanism that dynamically impacts the equilibrium free carriers far away from the photoexcited center (Fig. S1 in the supplementary material). At extended times, the bright and the dark signals decrease as the samples evolve toward the ground state.

Figure 4 plots the contrasts, extracted from the excited regions of the samples, against time delays. While these graphs agree well with their corresponding SUEM images, they reveal further details that highlight the differences in the dynamics. For instance, lightly doped p-type (A) silicon shows a positive signal right after optical excitation, whereas lightly doped n-type (B) silicon initially shows a negative signal ($\tau_1 = 5$ ps) that transitions into a positive right away. The time constants of the exponential rise in these samples are of the order of a few picoseconds, which is comparable to that in the intrinsic silicon (Table I). However, this increases in the heavily doped samples by at least an order of magnitude to 58 ps (p-type) and 77 ps (n-type). This suggests that the driving force for the emergence of the contrast changes dramatically as the doping type and concentration change. Furthermore, there is a sudden reduction in the signal after intensities maximize, which is more apparent and sharper in the heavily doped samples. Specifically, the time constants of these exponential decays decrease from 148 ps (p-type) and 146 ps (n-type) for lightly doped samples to 36 ps (p-type) and 10 ps (n-type) for heavily doped samples. The slow recovery, which appears to be faster than in the intrinsic silicon, is of the same order for all these cases.

To further explain the experimental observation, we present a numerical model that accounts for the doping dependent dynamics. This model considers the drift and diffusion processes generated by the intrinsic fields or those induced by photoexcitation. Generally, the optical excitation generates electron-hole pairs ($n^*_{e,h}$) in the sample, whose densities are determined by

$$n^*_{e,h} = \left(\frac{1}{2\pi w^2} e^{-(x^2+y^2)/2w^2}\right), \frac{\alpha(1-R)}{E} I_0 e^{-z\alpha}, \tag{3}$$

where w is the beam waist, I_0 is the laser intensity, R is the reflectivity of the surface, α is the absorption coefficient, and E is the photon energy. For the conditions used in this study, this

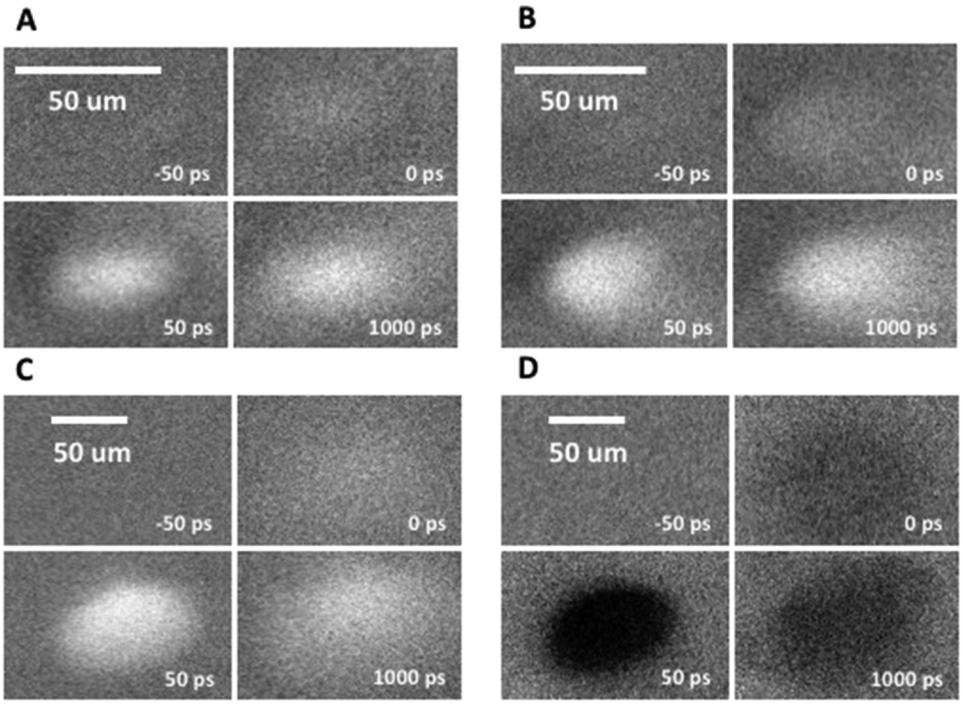

FIG. 3. (a) SUEM images recorded before ($t = -50$ ps) and after optical excitation ($t > 0$ ps) for lightly doped p-type (a), lightly doped n-type (b), heavily doped p-type (c), and heavily doped n-type (d) silicon. The bright contrast, emerging after optical excitation in the first three samples (a)–(c), is indicative of increased electron densities, while the dark contrast observed in the last sample (d) corresponds to the increased hole density.

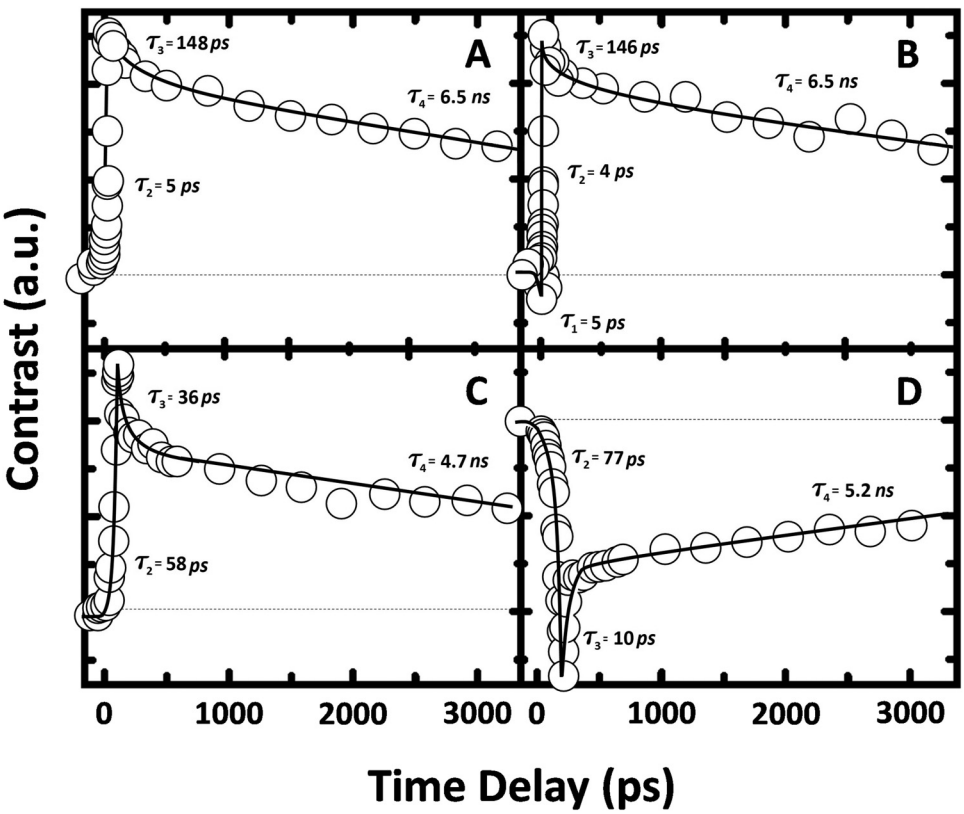

FIG. 4. The transient contrasts extracted from the photoexcited regions of lightly doped p-type (a), lightly doped n-type (b), heavily doped p-type (c), and heavily doped n-type (d) silicon. The dotted lines represent the baseline contrast.

translates to $\sim 10^{19}\,\mathrm{cm}^{-3}$ of free carriers in the samples. We have previously shown that these hot carriers initially undergo isotropic superdiffusion with the diffusion coefficient at least 3 orders of magnitude larger than that of the room temperature.[10] We have attributed this to the pressure increase in the excited volume that decays exponentially as carriers cool down.

To model the transport, we first write the transport equations by including the drift and diffusion of the photoexcited electrons and holes as

$$\frac{\partial n_e^*}{\partial t} + \nabla \cdot \left(D_e \nabla n_e^* - \mu_e n_e^* \nabla V \right) = 0, \tag{4}$$

$$\frac{\partial n_h^*}{\partial t} + \nabla \cdot \left(D_h \nabla n_h^* - \mu_h n_h^* \nabla V \right) = 0, \tag{5}$$

where D_e and D_h are the superdiffusion coefficients that exponentially decay with time to the room temperature diffusion coefficient. To increase the accuracy of our model, we also include the effect that the transport of the photoexcited carriers have on the background equilibrium carriers ($n_{e,h}$) generated by the initial doping. We assume a uniform doping in the samples as well as the complete ionization of the dopants at room temperature. Since these carriers are at room temperature, we ignore the diffusion term and write the transport equations as

$$\frac{\partial n_e}{\partial t} - \nabla \cdot (\mu_e n_e \nabla V) = 0, \tag{6}$$

$$\frac{\partial n_h}{\partial t} - \nabla \cdot (\mu_h n_h \nabla V) = 0. \tag{7}$$

In addition, to get the dynamics of the electric potential resulting from charge interactions, we write the Poisson equation:

$$\nabla^2 V = -\frac{(n_e^{total} - n_h^{total})}{\epsilon_0 \epsilon_r}, \tag{8}$$

where n_e^{total} and n_h^{total} are the sums of photoexcited and equilibrium electrons and holes, respectively, ϵ_0 is the vacuum permittivity, and ϵ is the relative primitively of the semiconductor. We simultaneously solve Eqs. (3)–(8) using the finite element method for a three-dimensional geometry ($1000 \times 1000 \times 200\,\mu\mathrm{m}^3$), which is excited at the center with a Gaussian laser pulse ($\sigma^2 = 25\,\mu\mathrm{m} \times 35\,\mu\mathrm{m}$, $\tau_p = 1\,\mathrm{ps}$) that exponentially decays into the bulk according to $I_0 e^{-z\alpha}$. In intrinsic and lightly doped samples, carriers are assumed to cool down by 1 ps after photoexcitation; however, for heavily doped samples, this value increases to a few picoseconds due to the bottlenecking of carrier-phonon scattering which becomes significant at large excitation densities.[17] For simplicity, we ignore the surface and bulk recombination that are usually slower than the time scale of our experiments.

Figure 5 plots the net carrier ($n_e^{total} - n_h^{total}$) intensities at the top 10 nm of the surfaces of heavily doped p-type (A) and n-type (B) silicon for various time delays. These examples showcase the extreme scenarios where the net transport is highly influenced by doping. In the p-type sample, the transport of carriers results in electron accumulation near the surface; this trend continues and maximizes by approximately 90 ps, after which the intensity reduces as carriers diffuse into the bulk. In n-type silicon, an opposite behavior emerges where holes accumulate near the surface, peaking at approximately 150 ps. This delay is due to the heavier effective masses of holes that slows their transport velocity.

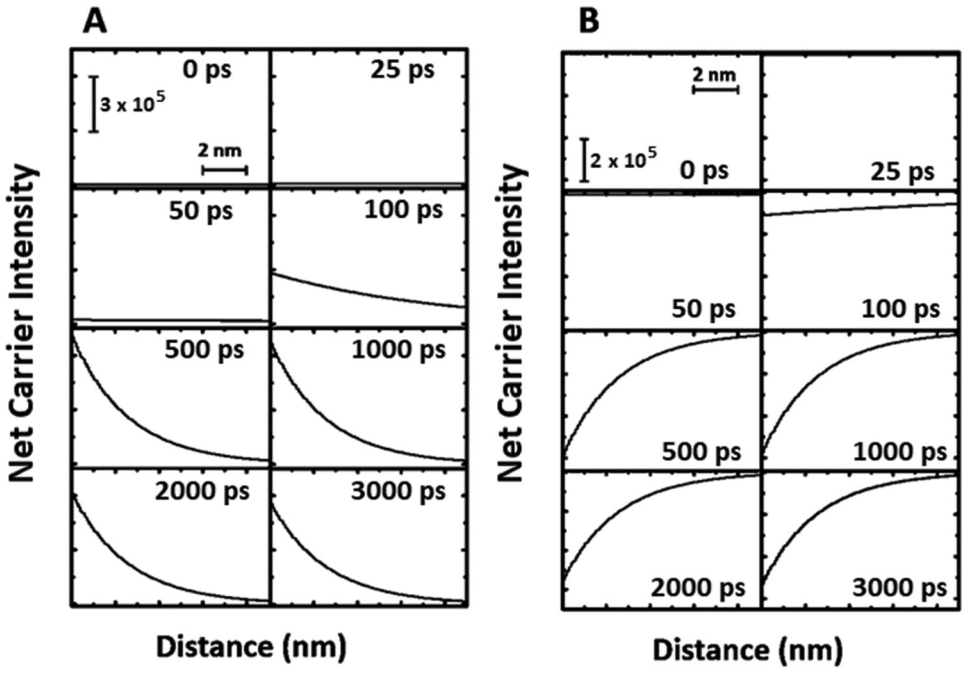

FIG. 5. Net carrier ($n_e - n_h$) intensities calculated for the top 10 nm of the surface in heavily doped p-type (a) and n-type silicon (b).

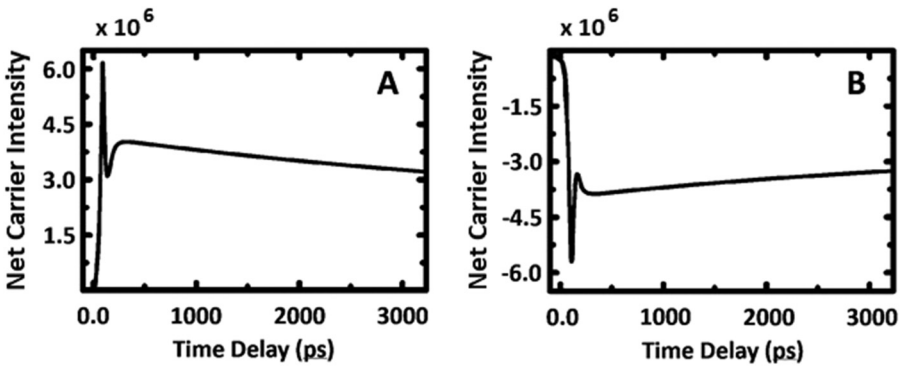

FIG. 6. Temporal evolution of the net carrier intensity for heavily doped p-type (a) and n-type (b) silicon, obtained from numerical simulation and averaged over the top 5 nm of the surface.

At extended times, when carriers have cooled down, room temperature diffusion takes over, driving the diffusion of carriers into the bulk.

Figure 6 plots the net carrier intensity averaged over the top 5 nm of the surfaces of heavily doped p-type (A) and n-type (B) silicon. These graphs, which agree relatively well with the experimental data, show systematics increases in the net electrons and holes on the surfaces of the p-type and n-type samples, respectively, primarily because of the built-in potential in the subsurface which separates the photoexcited electrons and holes and drifts them in opposite directions. Once the concentration of these carriers on the surface reaches a critical threshold, the Coulomb repulsion takes over and suddenly widens the distributions. Once these carriers are sufficiently separated and have completely cooled down, normal diffusion takes over to recover the ground state. The model also mimics the experimental results for intrinsic and lightly doped samples relatively well; it also accounts for the observation of the halos around the bright contrasts (Fig. S2 in the supplementary material). The simulation attributes the origin of these halos to the strong interaction between the photoexcited and equilibrium free carriers. This is because, after photoexcitation, electrons are driven away from the surface into the bulk faster than holes due to their lighter effective mass. Thus, the surface at the crossover becomes positive, inducing a radial electric field parallel to the surface. This drifts the free equilibrium electrons, which are abundant in intrinsic and lightly doped n-type silicon, from the surrounding to the crossover. This causes the crossover to become negative but quickly transition into positive by the surrounding electrons.

In conclusion, the space-time imaging of carrier dynamics at the surfaces and interfaces has the immense potential to unravel complex mechanisms of carrier transport, with the sub-picosecond temporal and nanometer spatial resolutions. In this study, the non-equilibrium carrier dynamics on the silicon surface show a strong dependence on the doping type and concentration. While such behavior is usually attributed to SPV, we show that the underlying mechanism is more complex and involves not only the photoexcited carriers but also the equilibrium free carriers in the samples. Such information helps paint a clear picture of surface-exclusive dynamics, which play a major role in the operation and performance of nanodevices.

SUPPLEMENTARY MATERIAL

In the supplementary material, we present experimental and numerical evidence for the formation of dark halos around the bright contrasts in intrinsic and lightly doped silicon (Fig. S1). Furthermore, we present a numerical simulation that shows the emergence of the dark contrast at early times that quickly transitions to bright contrasts at extended times (Fig. S2).

ACKNOWLEDGMENTS

This work was supported by the National Science Foundation (NSF) Grant No. DMR-0964886 and Air Force Office of Scientific Research Grant No. FA9550-11-1-0055 in the Physical Biology Center for Ultrafast Science and Technology at California Institute of Technology, which is supported by the Gordon and Betty Moore Foundation.

REFERENCES

[1]J. Shah, American Telephone and Telegraph Company, *Ultrafast Spectroscopy of Semiconductors and Semiconductor Nanostructures* (Springer, Berlin, New York, 1999).
[2]P. Hannaford, *Femtosecond Laser Spectroscopy* (Springer, New York, 2005).
[3]R. R. Alfano, *Semiconductors Probed by Ultrafast Laser Spectroscopy* (Academic Press, Orlando, FL, 1984).
[4]F. Bechstedt and R. Enderlein, *Semiconductor Surfaces and Interfaces: Their Atomic and Electronic Structures* (Akademie-Verlag, Berlin, 1988).
[5]W. Mönch, *Semiconductor Surfaces and Interfaces*, 3rd rev. ed. (Springer, Berlin, New York, 2001).
[6]J. L. Morán-López, *Physics of Low Dimensional Systems* (Kluwer Academic/Plenum Publishers, New York, 2001).
[7]E. N. Bolin Liao, "Scanning ultrafast electron microscopy: A novel technique to probe photocarrier dynamics with high spatial and temporal resolutions," Mater. Today Phys. **2**, 8 (2017).
[8]B. Liao, E. Najafi, H. Li, A. J. Minnich, and A. H. Zewail, "Photo-excited hot carrier dynamics in hydrogenated amorphous silicon imaged by 4D electron microscopy," Nat. Nanotechnol. **12**, 871 (2017).
[9]B. Liao, H. Zhao, E. Najafi, X. Yan, H. Tian, J. Tice, A. J. Minnich, H. Wang, and A. H. Zewail, "Spatial-temporal imaging of anisotropic photocarrier dynamics in black phosphorus," Nano Lett. **17**, 3675–3680 (2017).
[10]E. Najafi, V. Ivanov, A. Zewail, and M. Bernardi, "Super-diffusion of excited carriers in semiconductors," Nat. Commun. **8**, 15177 (2017).

[11]E. Najafi, T. D. Scarborough, J. Tang, and A. Zewail, "Ultrafast dynamics. Four-dimensional imaging of carrier interface dynamics in p-n junctions," Science **347**, 164–167 (2015).
[12]L. Kronik and Y. Shapira, "Surface photovoltage phenomena: Theory, experiment, and applications," Surf. Sci. Rep. **37**, 1–206 (1999).
[13]J. M. Marshall and D. Dimova-Malinovska, *Photovoltaic and Photoactive Materials: Properties, Technology, and Applications* (Kluwer Academic, Dordrecht, Boston, MA, 2002).
[14]C. J. R. Brunetti, F. Nava, L. Reggiani, G. Bosman, and R. J. J. Zijlstra, "Diffusion coefficient of electrons in silicon," J. Appl. Phys. **52**, 6713–6722 (1981).
[15]V. E. Cosslett, "Scanning electron-microscopy—Physics of image-formation and microanalysis," Nature **323**, 212–212 (1986).
[16]R. E. Lee, *Scanning Electron Microscopy and X-Ray Microanalysis* (Prentice Hall, Englewood Cliffs, NJ, 1993).
[17]F. Streicher, S. Sadewasser, and M. Lux-Steiner, "Surface photovoltage spectroscopy in a Kelvin probe force microscope under ultrahigh vacuum," Rev. Sci. Instrum. **80**, 013907 (2009).
[18]M. Arita, K. Torigoe, *et al.*, "Surface band-bending and fermi-level pinning in doped Si observed by Kelvin force microscopy," Appl. Phys. Lett. **104**(13), 132103 (2014).
[19]A. Van der Ziel, *Solid State Physical Electronics*, 3rd ed. (Prentice Hall, Englewood Cliffs, NJ, 1976).
[20]J. Cazaux, "Calculated influence of work function on SE escape probability and secondary electron emission yield," Appl. Surf. Sci. **257**, 1002–1009 (2010).
[21]Y. C. Yong and J. T. Thong, "Determination of secondary electron spectra from insulators," Scanning **22**, 161–166 (2000).
[22]P. A. Wolff, "Theory of secondary electron cascade in metals," Phys. Rev. **95**, 56–66 (1954).
[23]K. G. Mckay, "Secondary electron emission," Adv. Electron. **1**, 65–130 (1948).
[24]O. Hachenberg, W. Brauer, "Secondary electron emission from solids," Adv. Electron. Electron. Phys. **11**, 413–499 (1959).
[25]D. K. Schroder, "Carrier lifetime in silicon," IEEE Trans. Electr. Devices **44**(1), 160–170 (1997).
[26]J. Wagner, J. A. del Alamo, "Band-gap narrowing in heavily doped silicon: A comparison of optical and electrical data," J. Appl. Phys. **63**(2), 425–429 (1988).